Correction of non-random mutational biases along a linear bacterial chromosome by the mismatch repair endonuclease NucS

Oyut Dagva, Annabelle Thibessard, Jean-Noël Lorenzi, Victor Labat, Emilie Piotrowski, Nicolas Rouhier, Hannu Myllykallio, Pierre Leblond, Claire Bertrand

Nucleic Acids Research, 2024, 1–15
https://doi.org/10.1093/nar/gkae132
Genome integrity, repair and replication

Correction of non-random mutational biases along a linear bacterial chromosome by the mismatch repair endonuclease NucS

Oyut Dagva [1], Annabelle Thibessard [1], Jean-Noël Lorenzi [2], Victor Labat [1], Emilie Piotrowski [1], Nicolas Rouhier [3], Hannu Myllykallio [4], Pierre Leblond [1,*] and Claire Bertrand [1,*]

[1]Université de Lorraine, INRAE, UMR 1128 DynAMic, 54000 Nancy, France
[2]CNRS, Institut Jacques Monot, 75013 Paris, France
[3]Université de Lorraine, INRAE, UMR 1136 IAM, 54000 Nancy, France
[4]Ecole Polytechnique, INSERM U696-CNRS UMR 7645 LOB, 91128 Palaiseau, France

*To whom correspondence should be addressed. Tel: +33 3 72 74 51 44; Email: pierre.leblond@univ-lorraine.fr
Correspondence may also be addressed to Claire Bertrand. Tel: +33 3 72 74 51 89; Email: claire.bertrand@univ-lorraine.fr

Abstract

The linear chromosome of *Streptomyces* exhibits a highly compartmentalized structure with a conserved central region flanked by variable arms. As double strand break (DSB) repair mechanisms play a crucial role in shaping the genome plasticity of *Streptomyces*, we investigated the role of EndoMS/NucS, a recently characterized endonuclease involved in a non-canonical mismatch repair (MMR) mechanism in archaea and actinobacteria, that singularly corrects mismatches by creating a DSB. We showed that *Streptomyces* mutants lacking NucS display a marked colonial phenotype and a drastic increase in spontaneous mutation rate. *In vitro* biochemical assays revealed that NucS cooperates with the replication clamp to efficiently cleave G/T, G/G and T/T mismatched DNA by producing DSBs. These findings are consistent with the transition-shifted mutational spectrum observed in the mutant strains and reveal that NucS-dependent MMR specific task is to eliminate G/T mismatches generated by the DNA polymerase during replication. Interestingly, our data unveil a crescent-shaped distribution of the transition frequency from the replication origin towards the chromosomal ends, shedding light on a possible link between NucS-mediated DSBs and *Streptomyces* genome evolution.

Graphical abstract

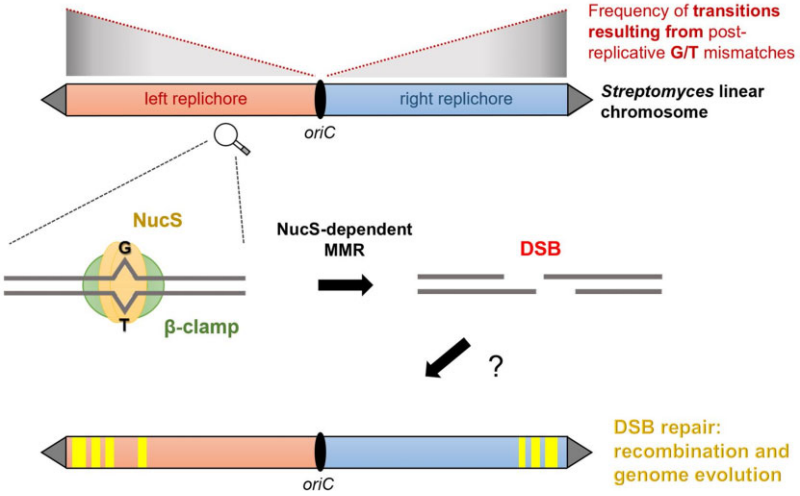

Introduction

In all organisms, the fidelity of DNA replication is crucial for the accurate transmission of genetic information. During replication, despite the accuracy of the DNA polymerase, base-pairing errors result in mismatches that are detected and corrected either by the proofreading 3′–5′ exonuclease activity of the DNA polymerase or by the post-replicative mismatch repair (MMR) (1). The canonical MMR system has been extensively studied in *Escherichia coli* and is well characterized both biochemically and genetically (2). Methyl-directed MMR (MutSL dependent) in *E. coli* uses transient DNA hemimethylation to identify the daughter strand and excise the

Received: December 21, 2023. **Revised:** January 19, 2024. **Editorial Decision:** February 7, 2024. **Accepted:** February 9, 2024

mismatched nucleotide(s). The DNA repair process is subsequently completed by a template-dependent re-synthesis in order to restore the original genetic information (3). MMR deficient *E. coli* mutants exhibit a 100- to 1,000-fold increase in mutation rate resulting in a hypermutable phenotype (4). Although the canonical MMR system is widespread, bioinformatic studies surprisingly failed to identify homologs of the *mutSL* genes in the genomes of many archaeal species and of almost all members of the actinobacteria phylum (5). However, these organisms exhibit a mutation rate comparable to that of canonical MMR-bearing bacterial species (6,7), suggesting the existence of an alternative MMR pathway.

NucS, discovered in the archaeon *Pyrococcus abyssi*, was reported as a novel endonuclease that degrades single-stranded regions on branched DNA (8). Structural analysis of *P. abyssi* NucS revealed a two-domain enzyme that adopts a dimeric conformation. The N-terminal domain is involved in dimerization and DNA binding, while the C-terminal domain carries a minimal RecB-like domain and contains the catalytic site (8). A recent study identified the orthologs of NucS, named EndoMS (mismatch-specific endonuclease) from the hyperthermophilic euryarchaea *Pyrococcus furiosus* and *Thermococcus kodakarensis*, which specifically recognizes double-stranded DNA (dsDNA) containing a mismatch (9). Strikingly, biochemical characterization revealed that EndoMS from *T. kodakarensis* introduces double-strand breaks (DSBs) by cleaving both strands of mismatched substrates. While dsDNA containing G/T, G/G, T/T, T/C and A/G mismatches is cleaved with variable efficiency, no activity on A/C, C/C and A/A mispairs is detected *in vitro*. This endonuclease activity is considerably enhanced by the association with the sliding clamp PCNA (proliferating cell nuclear antigen). Sliding clamps are found in all organisms and are considered to be a universal platform that recruits numerous DNA-processing enzymes during replication and repair (10,11). In *E. coli*, the replication clamp interacts with MutS and MutL, as well as with the DNA polymerase III, suggesting a coupling between DNA replication and MMR (12,13). NucS was in fact historically discovered as an interacting partner of PCNA in *P. abyssi* (14) and this interaction modulates NucS structure and activity (8,15). *P. abyssi* NucS and *T. kodakarensis* EndoMS exhibit a PCNA-interacting protein (PIP) box in their C-terminal domain (14). A similar box is also known as the clamp-binding motif CBM in bacteria and has a general [EK]-[LY]-[TR]-L-F consensus sequence that tolerates greater variability than the PIP-box (16). The crystal structure elucidation of EndoMS dimer with dsDNA confirmed a preferred binding to specific mismatches and a preliminary complex model with PCNA was proposed (17). This interaction of a restriction enzyme with the sliding clamp is a remarkable specificity that has never been reported before.

In actinobacteria, the biological role and the enzymatic activity of EndoMS/NucS (referred to as NucS hereafter) have been mainly studied in *Mycobacterium* species and *Corynebacterium glutamicum*. Deletion of *nucS* in *Mycobacterium smegmatis* and in *C. glutamicum* leads to the increase of spontaneous mutation rates and causes a transition-biased mutation spectrum, highlighting its role in mutation avoidance (18–22). Cleavage assays have shown that NucS of *C. glutamicum*, like archaeal enzymes, generates a DSB by preferentially cleaving G/T mismatched DNA substrate. The activity of the enzyme is dependent on the presence of divalent cation cofactors, Mn^{2+} or Mg^{2+}, and its efficiency is greatly enhanced by the addition of β-clamp, the bacterial homolog of PCNA. However, such cleavage has not yet been demonstrated in *Mycobacterium* species. Taken together, these results suggest that NucS corrects mismatches that have escaped the proofreading activity of the polymerase and represents an important component of the non-canonical MMR system. Most importantly, unlike the canonical MMR, NucS creates a DSB that, if left unprocessed, should be dangerous to the cell. DSBs are indeed the most detrimental type of DNA damage in all living cells (23). They can be repaired by homologous recombination when a DNA template is available or by illegitimate recombination for which a homologous template is not necessary (24–26). How the DSB induced by NucS during MMR is repaired and how the correct base pair is restored has yet to be elucidated.

Streptomyces are soil bacteria belonging to the phylum of actinobacteria and are known as the most prolific producers of specialized metabolites used in medicine and other industries (27). These bacteria have original genomic features including a high GC content (∼72%) and a large linear chromosome (6–12 Mb) ended by terminal inverted repeats (TIR). The genome of *Streptomyces* is highly compartmentalized with a conserved central region flanked by variable chromosomal arms (28,29). Preliminary genomic comparison studies revealed that the loss of synteny at the terminal arms results from DNA insertions and deletions (30). Recently, a more comprehensive analysis performed on 125 *Streptomyces* genomes highlighted that the great flexibility of the chromosomal arms is due to gain and loss of genes resulting from horizontal gene transfer or genome shuffling (29). This phenomenon is directly linked to large genomic rearrangements spontaneously occurring in the arms, including large deletions (up to 2 Mb), chromosome circularization and arm replacement events (31–34). Recent work has shown that repair of DSBs in the chromosomal arms resulted in all the chromosomal rearrangements observed in the spontaneous variants (35). DSBs in *Streptomyces* can be repaired by homologous recombination but also by non-homologous end-joining (NHEJ), a widespread illegitimate recombination mechanism among eukaryotes that is not ubiquitous in bacteria (35–38). The repair of DSBs in the central part of the chromosome can be mutagenic when mediated by NHEJ, with deletions of up to 20 kb, whereas repair at the terminal regions can result in huge genomic alterations such as deletions of up to 2.1 Mb, or arm replacement (mediated by a single crossing-over between two homologous sequences present in both arms, or by break-induced replication events). Some scar analyses revealed insertion events of ectopic sequences ranging from tens to thousands of nucleotides, highlighting possibilities of potential integration of foreign DNA in a natural environment. Therefore, DSB repair has been proposed as a driving force for the huge plasticity and evolution of *Streptomyces* genome. Various exogenous sources such as UV light, ionizing radiation or mutagenic chemicals can induce DSBs, but vast amount of these are thought to arise from internal cellular processes, for instance during DNA synthesis when the replication fork collapses (39–41). The recent discovery of the non-canonical MMR unveils a new putative internal origin of DSBs that could have a role in *Streptomyces* genome plasticity. In this study, we used mutation accumulation experiment to demonstrate the role of NucS in mutation avoidance in *Streptomyces ambofaciens* and we showed the enzyme cleavage activity on diverse base pair mismatches, particularly on G/Ts, generating a DSB. Our results notably

highlight a transition bias that increases from the replication origin towards the extremities of the chromosome of strains lacking NucS, suggesting that the non-canonical MMR system is more active in the terminal regions of *Streptomyces* linear chromosome.

Materials and methods

Strains, plasmids and growth conditions

DH5α *E. coli* strain was used as the cloning host for plasmid construction. Plasmid pGEM®-T Easy (Promega) was used as a primary cloning vector. *E. coli* BL21 (DE3) strain was used for *nucS* and *dnaN* heterologous expression. Plasmid pET15B is the expression vector used in this study, and pSBET is a helper plasmid for heterologous expression. *E. coli* ET12567 pUZ8002 was used as a donor for intergeneric conjugation to introduce DNA constructs into *S. ambofaciens*. Plasmid pUZ8002 carries the conjugative functions. *E. coli* strains were grown in Luria-Bertani (LB) medium at 37°C, except for the BW25113 pKD20 thermosensitive strain used for PCR targeting which was grown at 30°C. Plasmid pKD20 expresses the phage λ Red recombination system. The pOSV508 plasmid allowing the expression of *int* and *xis* from pSAM2 (42) is used in *Streptomyces* to excise genetic cassettes by site-specific recombination. The integrative plasmid pSET152 is used for complementation in *Streptomyces*. The *Streptomyces* mutants mentioned in this study were derived from our reference strain *S. ambofaciens* ATCC23877. *S. ambofaciens* strains were grown on Soya Flour Mannitol agar (SFM) for spore harvest. Single colony isolation for phenotypic observation and growth for DNA extraction were performed on Hickey-Tresner (HT) agar and liquid medium, respectively.

Deletion of *nucS* in *S. ambofaciens*

The *nucS*-deficient mutants were generated by PCR targeting (43). Briefly, the deletion was carried out in a recombinant bacterial artificial chromosome (BAC) containing a 35 kb region containing *nucS* gene, which was replaced by an *oriT-aac(3)IV* apramycin resistance cassette using the lambda-red system in the highly recombinogenic *E. coli* BW25113/pKD20 strain. This recombinant BAC was then conjugated into *S. ambofaciens* using, as a donor strain, the non-methylating *E. coli* ET12567 which harbors the mobilizing pUZ8002 plasmid. Double-crossover events leading to the replacement of genomic *nucS* by the cassette were monitored by screening for both apramycin resistance and kanamycin sensitivity (selection of the loss of the BAC vector). As the disruption cassette is flanked by pSAM2 *attL* and *attR* sites, its excision by site-specific recombination can be induced thanks to the introduction of pOSV508 plasmid allowing the expression of *int* and *xis* from pSAM2 (42). The excision event was verified by PCR in the exconjugants. The Δ*nucS*-1 and Δ*nucS*-2 mutants originate from two well-isolated colonies of the same conjugation experiment, whereas Δ*nucS*-3 and Δ*nucS*-4 mutants originate from a second conjugation. These two conjugations were performed with two modified BACs. The resulting four *nucS*-deficient strains were therefore considered as independent.

Complementation of Δ*nucS* mutants

S. ambofaciens nucS locus (SAM23877_5135) including the promoter and the coding region was amplified by PCR using primers nucS_compl_F/R containing an EcoRI restriction site (Supplementary Table S1). The PCR fragment was ligated into the pGEM-T Easy vector, sequenced and then released by EcoRI digestion in order to be inserted into the conjugative and integrative plasmid pSET152, resulting in the pSET152-*nucS* complementation vector. The latter was introduced into the four Δ*nucS* mutants by intergeneric conjugation as described above. As pSET152 plasmid is integrative at the φC31 chromosomal *attB* site, there is only one complementation copy of *nucS* gene per chromosome. The integration of the pSET152-*nucS* plasmid in the chromosome was verified by PCR.

Estimation of mutation rate by fluctuation tests

Spontaneous mutation rates were estimated using fluctuation assays (44). Isolated colonies of wild-type (WT) and Δ*nucS*-2 strains were excised after 7 and 5 days of growth on SFM at 30°C, respectively, and vortexed vigorously in water to homogenize spores in solution. Three volumes of 100 µl of each suspension were plated on three SFM plates supplemented with rifampicin (50 µg/ml) and appropriate dilutions were plated on SFM in order to determine the total viable cell number. Rifampicin-resistant colonies were counted after 4 days of incubation at 30°C. The mutation rate was determined using the Ma-Sandri-Sarkar maximum likelihood method (45) and confidence intervals were calculated according to the literature (46). These calculations were performed using the FALCOR web tool available at https://lianglab.brocku.ca/FALCOR/ (47).

Heterologous expression and purification of His-tagged $NucS_{Sam}$ and β-$clamp_{Sam}$ proteins

The coding sequences of *nucS* (SAM23877_5135) and of *dnaN* (SAM23877_3780), which code for $NucS_{Sam}$ and β-$clamp_{Sam}$, respectively, were amplified by PCR from *S. ambofaciens* chromosome. The amplification of *nucS* and *dnaN* was carried out with the primer couples nucS_F/R and dnaN_F/R, respectively (Supplementary Table S1). The PCR fragments were ligated into the pGEM®-T Easy vector and were verified by sequencing. The digestion by NdeI and BamHI released *nucS* and *dnaN* sequences, which were further cloned into the pET15b expression vector. Using these constructs, a His-tag is added to the N-terminal end of $NucS_{Sam}$ and β-$clamp_{Sam}$. The *E. coli* BL21 (DE3) strain, containing the helper plasmid pSBET (48), was used for protein expression. Expression and purification of $NucS_{Sam}$ and β-$clamp_{Sam}$ were performed using the same procedure. Bacteria were grown at 37°C to exponential phase in LB medium supplemented with 50 µg/ml kanamycin and 100 µg/ml ampicillin. The expression of chaperones was boosted by adding ethanol to the bacterial culture to a final concentration of 0.5% and by cooling it at 4°C for 3 h. IPTG was then added to a final concentration of 100 µM and cells were further grown for 20 h at 20°C. Cells were collected, diluted in buffer A (30 mM pH 8.0 Tris–HCl, 200 mM NaCl, 10 mM imidazole, 0.05% polyethyleneimine) and disrupted by sonication. The soluble extract was applied to an IMAC-Select affinity gel column (Sigma Aldrich, St. Louis, MO, USA) equilibrated in buffer A. After extensive washing, the protein was eluted using the same buffer A with an imidazole concentration of 100 mM. Fractions containing the protein of interest were pooled, concentrated using an Amicon centrifugal filter (Millipore) with a 10 kDa cut-off and

loaded onto a Superdex 200 pg HiLoad 16/600 (GE Healthcare, 1 ml/min). Sample purity was assessed by 12% SDS-PAGE analysis and sample concentration was determined by spectrophotometry using a theoretical molar extinction coefficient at 280 nm of 20 190 M^{-1} cm^{-1} and 19 940 M^{-1} cm^{-1} for $NucS_{Sam}$ and β-$clamp_{Sam}$, respectively.

Cleavage assay

Heteroduplex DNA was prepared by annealing oligonucleotides at 95°C for 10 min. The sequence and the different combinations of oligonucleotides are shown in Supplementary Table S2. The cleavage reaction of the ds-DNA substrate was generally performed at 30°C for 60 min in a buffer containing 2.4 μM $NucS_{Sam}$ and/or 1.2 μM β-$clamp_{Sam}$, 25 mM Bis–Tris pH 6.4, 2.5 mM $MnCl_2$, 0.1% Triton X-100. For cleavage reaction performed with Mg^{2+}, either 2.5 mM $MnCl_2$ was replaced by 2.5 mM $MgCl_2$ in the above conditions, or the reaction conditions described by Takemoto *et al.* (21) were used as follows, 20 mM Tris–HCl, pH 8.0, 2.5 or 10 mM $MgCl_2$, 4 mM dithiothreitol, 0.071 mg/ml BSA and 30 or 100 mM K[oAc]. Monomeric $NucS_{Sam}$ fraction was used in these assays. The products were analyzed by 10% native PAGE. At least three biological replicates were done for each mismatch configuration.

Mutation accumulation experiments

The WT strain and the four independent *nucS*-deficient mutants were used for mutation accumulation (MA) experiments. Three lineages per Δ*nucS* mutants and 12 WT lines were generated. Each line was generated by streaking a single colony. A sporulation cycle was initiated by streaking a single well-isolated colony from each lineage onto a new SFM plate and incubating at 30°C for 7 days. This procedure was repeated every week for 60 cycles. To keep track of evolved lineages, colonies streaked at each new cycle were picked from the agar plate, resuspended in 20% glycerol and stored at –20°C.

Genomic DNA preparation and whole genome sequencing analysis

Parental and evolved strains at the end of the 60th sporulation cycle were grown in liquid HT medium to extract genomic DNA (49). Whole genome sequencing was performed using an Illumina Genome Analyzer to obtain 300-bp paired-end reads (Mutualized Platform for Microbiology (P2M), Pasteur Institute, Paris). Data analysis was performed using Geneious Prime 2023.2.1. Reads from each lineage were trimmed based on their quality (minimum quality = 20; primers, indexes and reads less than 20 bp in length were removed). Trimmed reads from parental strains only were mapped to the *S. ambofaciens* ATCC23877 reference genome (GenBank: CP012382.1) using Geneious mapper with the following parameters: sensitivity = 'medium-low', fine tuning = 'iterate up to 5 times', minimum mapping quality = '30', only map paired reads which = 'map closely nearby'. The mean depth coverage of each assembly ranged from 113× to 481×. Consensus sequence was generated from alignments using the highest quality parameter as a threshold and 'N' was assigned to sites with coverage <20. Annotation was performed with Prokka (50) using a custom database containing all the genes from *S. ambofaciens* ATCC 23877 chromosome. These annotated genomes were then used as references for mapping trimmed reads from evolved lines. The same Geneious alignment settings as above were applied. The mean depth coverage of each mapping ranged from 45× to 565×. Variant calling was performed using the in-built 'Find Variations/SNPs' feature. A single-nucleotide polymorphism (SNP) was called if the position was covered by at least 20 reads, was found at a frequency of at least 0.9, and was not found in a niche (>3 SNPs in a sliding 100-bp window with a 1-bp step size). For a duplicated sequence, the frequency of at least 0.9 would not be observed if only one of the two copies carries the SNP, and if the two copies carry it, the calling could not be assigned to any of them. For this reason, all the genomic analyses were done on the whole genome of *S. ambofaciens* ATCC23877 with the exception of repeated sequences, including the 200 kb long TIR of *S. ambofaciens*. Note that 89 kb circular plasmid pSAM1 was also excluded from the analyses. Therefore, in the manuscript, when we refer to the chromosome, it is without the above sequences.

Genomic comparison of *Streptomyces* close environmental strains

Genomes of RLB1-8 and RLB3-17 (accession numbers CP041650 and CP041610, respectively) environmental strains (51) were used in this study. ANIb (Average Nucleotide Identity using BLAST) was calculated between both genomes: we averaged the two reciprocally obtained ANIb scores (52). For transition analysis in whole genome, both sequences were aligned using the progressive Mauve algorithm (53). The SNP call table was exported with MAUVE tool 'export SNPs'. For transition analyses in coding sequences, both genome sequences were annotated using RAST (54), with the RAST pipeline (https://rast.nmpdr.org/) using RASTtk (v1.3.0) with all parameters by default. After extraction, RAST annotations (with GenBank files) were formatted to a usable format for the subsequent pipeline. BLASTp was performed between each gene coding for a protein of one genome against that of the other genome and reciprocally. Orthologs were defined by identifying BLASTp reciprocal best hits (BBH) with at least 40% identity, 70% coverage, and an *E*-value lower than 1e-10. For each orthologous gene pair, the nucleotide sequences of both genes were retrieved and aligned with MAFFT (55). In these alignments (one per orthologous gene pair), identified non-gap differences corresponded to SNPs. RLB1-8 genome was used as reference. The sequence of the five identified integrative and conjugative elements present in RLB1-8 genome (56) were removed from the transition analysis to avoid bias caused by their possible redundant nucleotide sequences. The 357 kb TIR of RLB1-8 genome was also excluded, as in the MA study.

Statistical analyses of mutation distribution along the chromosome

For the analyses of mutation distribution along the chromosome, the number of mutations was counted within a sliding non-overlapping 100 kb window, starting from the replication origin *oriC*, extending towards the left or the right end of the chromosome. The number in windows of the right replichore was added to the number in windows at the same distance of *oriC* in the left replichore. The sum was represented as a function of the distance from *oriC*. As the left replichore is slightly longer than the right one in both *S. ambofaciens* ATCC23877 and RLB1-8 genomes, values corresponding to

the last 100 kb windows at the extremity of the left replichore were excluded from the analyses. Correlation analyses between the number of mutations and the distance from the origin of replication in the genomes of evolved lines or between the genomes of environmental strains were done with R software (https://www.R-project.org/). Pearson correlation test was used when the distribution of the residues was compatible with the normal low and Kendall'T coefficient was calculated when the distribution of the residues was not compatible with the normal low.

Reagents

All cloning reagents, including restriction enzymes (FastDigest), T4 DNA ligase, and DNA polymerases (DreamTaq, Phusion) were provided by Thermo Fisher Scientific. All molecular biology kits (PCR purification, gel extraction and plasmid miniprep) were also provided by Thermo Fisher Scientific.

Results

NucS is highly conserved in *Streptomyces*

The persistence of *nucS* across *Streptomyces* genus was determined by searching for *nucS* orthologs in the genomes of a collection of 125 species representative of the genus diversity (29). A single copy of *nucS* was present in all species and, as every core gene, is localized in the central region of the chromosome. NucS protein sequence consists of 223 amino acids and is highly conserved with identities ranging from 86% to 97% when using NucS from *S. ambofaciens* ($NucS_{Sam}$) as a reference. The ubiquity of *nucS* through *Streptomyces* genus suggests its important role in cell development and survival in *Streptomyces*. When compared to NucS from *M. smegmatis* and *Mycobacterium tuberculosis* (18), or from *C. glutamicum* (20) the identity drops to 75%, 78%, and 72% respectively, highlighting the significant conservation of the protein among actinobacteria. $NucS_{Sam}$ shares structural homologies with NucS from *P. abyssi* (8), bearing an N-terminal DNA binding domain connected by a linker to the C-terminal RecB-like nuclease domain. The well-known RecB motifs for nuclease activity are present in $NucS_{Sam}$ and most importantly all the catalytic residues are conserved across actinobacteria (Supplementary Figure S1). The consensus clamp-binding KLRLF motif is also present in the C-terminal part of all *Streptomyces* NucS proteins. These data strongly suggest that $NucS_{Sam}$ may have a similar activity to $NucS_{Pab}$.

$NucS_{Sam}$ is involved in mutation avoidance

To assess the effect of *nucS* deletion, four independent mutants deleted for *nucS* (Δ*nucS*) were generated by PCR targeting method in *S. ambofaciens* ATCC 23877 strain. For each independent Δ*nucS* mutant, a complemented strain, expressing *nucS* WT copy under the control of its own promoter, was obtained using the integrative plasmid pSET152. The Δ*nucS* mutants were grown for 8 days at 30°C on HT solid medium for phenotype analysis. Compared to the WT, all *nucS*-deleted strains shared the same remarkable phenotype consisting of a high frequency of sectorized colonies in their progeny (Figure 1A and B). This phenotype is heritable. The proportion of sector-harboring colonies was quantified in the 4 independent Δ*nucS* mutants, in the WT and in the complemented strains. The occurrence of sectorized colonies was significantly greater in Δ*nucS* strains compared to the WT strain (overall 82% versus 7% respectively; Z-test for proportions with Bonferroni correction, $P < 10^{-3}$; Figure 1C). In the complemented strains, this frequency was drastically reduced to levels comparable to those of the WT (on average 9% versus 7% respectively). This indicates that expressing *nucS* behind its original promoter restored the WT phenotype. In the WT background, it has been shown that the spontaneous variability of the colonial phenotype originates from mutations, affecting phenotypical traits in *Streptomyces* such as pigmentation or sporulation (31,57). We therefore assumed that the specific phenotype observed for *nucS*-defective strains was the result of mutation accumulation.

To confirm that *nucS* deletion results in a hypermutator phenotype, the spontaneous emergence of rifampicin-resistant colonies was monitored by fluctuation assays. Originally described by Luria and Delbruck (44), fluctuation tests are widely used for estimating mutation rates. As all 4 Δ*nucS* strains exhibited the same colonial phenotype, Δ*nucS*-2 was selected for further assays. The same procedure was applied to the corresponding complemented strain. Deletion of *nucS* resulted in an increase in mutation rate by a 130-factor compared to the WT strain (1.63×10^{-6} versus 1.24×10^{-8} mutations per cell, respectively, Figure 1D). Of note, a mutation rate comparable to that of the WT strain was recovered in the complemented strain (1.24×10^{-8} versus 1.08×10^{-8} mutations per cell, respectively) confirming that the absence of NucS was responsible for the observed increase in the mutation rate. Similar findings were reported in *Streptomyces coelicolor*, in which inactivation of *nucS* resulted in a 2-log increase in mutation rate, although no colonial phenotype was reported in this study (18). Altogether, these results showed that *nucS* inactivation caused a hypermutator phenotype and highlighted the key role of NucS in mutation avoidance.

Purification of His-tagged $NucS_{Sam}$ and His-tagged β-$clamp_{Sam}$ proteins

NucS from the actinobacterium *C. glutamicum* has been recently demonstrated as capable of cleaving mismatched dsDNA (20,21). Yet, Castañeda-García and colleagues (18) have shown that NucS from *M. smegmatis* has ssDNA-binding activity but no cleavage activity was detected neither on ssDNA nor on mismatched dsDNA. For this reason, the activity of $NucS_{Sam}$ *in vitro* was investigated. To achieve this, we purified N-terminal His-tagged $NucS_{Sam}$ by cloning the *nucS* coding sequence (SAM23877_5135) in the pET15b expression vector for heterologous expression in *E. coli* BL21. The fusion protein was purified using affinity chromatography and gel filtration. Based on the amino acid sequence, the calculated molecular weight of the protein is 24762.44 Da. The gel filtration chromatogram showed a main peak at an elution volume corresponding to an estimated molecular weight of 41 kDa (Supplementary Figure S2). Additional peaks were observed with estimated molecular weights of 61 and 115 kDa, indicating the presence of multimeric forms. Because it was difficult to firmly conclude about the oligomerization state of the major form of purified $NucS_{Sam}$, the fractions corresponding to the main peak were collected and subjected to size exclusion chromatography coupled with multi-angle light scattering (SEC-MALS). The analysis revealed two main peaks with molecular weights of 30 026 Da and 61 151 Da, which would correspond to monomeric and dimeric forms of $NucS_{Sam}$, respectively. Because the homogeneity of these peaks was moder-

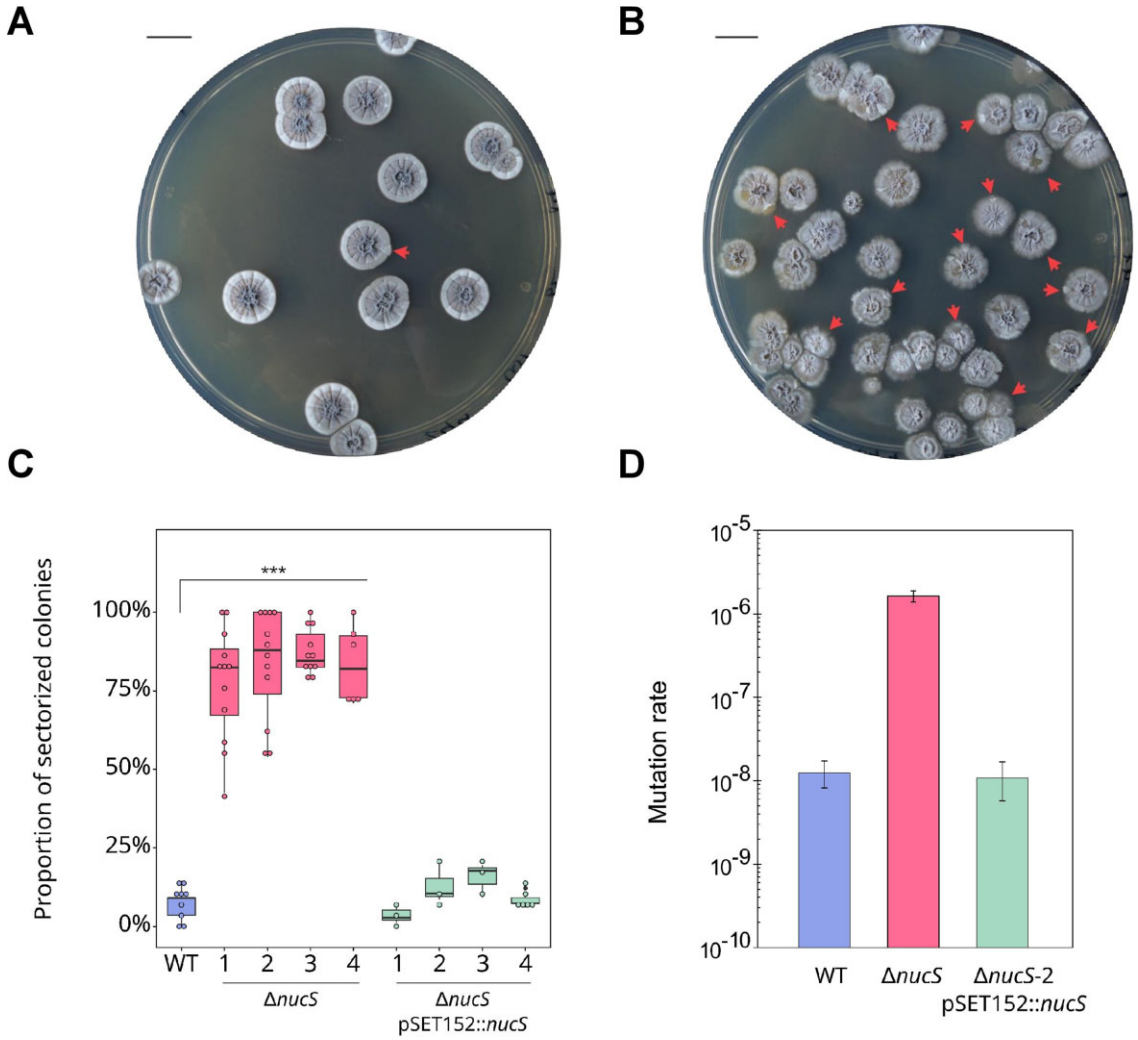

Figure 1. Colonial phenotype of *nucS*-deleted mutants. (**A**) *S. ambofaciens* WT strain and (**B**) Δ*nucS* mutant were grown on HT agar for 8 days at 30°C. A sectorized colonial phenotype was observed for *nucS*-deleted strain (red arrows). Scale bar represents 1 cm. (**C**) Proportion of sector-harboring colonies counted in the WT (blue), the four independent Δ*nucS* mutants (pink) and in their complemented strains denoted as Δ*nucS* pSET152::*nucS* (green) (z-test for proportions with Bonferroni correction, ***$P < 0.001$). (**D**) The rate of spontaneous mutations conferring rifampicin resistance was determined by fluctuation assay in WT, Δ*nucS*-2 and its complemented strain Δ*nucS-2* pSET152::*nucS*. Error bars represent 95% confidence intervals.

ate, molecular weights were determined considering the right side of the peaks. The gel filtration profile and SEC-MALS analysis indicate that the protein may exist in an equilibrium between a monomeric and dimeric state, with the monomeric form being more prevalent under the purification conditions employed in this work. *C. glutamicum* NucS is also found as a monomer and as a dimer in solution, with a majority of dimeric forms (20). One hypothesis is that the assembly of two monomers into a dimer could be stimulated by the presence of a DNA substrate. However, *in vitro* studies have never shown the presence of NucS in monomeric form for archaeal enzymes, suggesting that DNA substrate is not necessary for dimerization (8,9,17).

The processivity-promoting factor β-clamp from *S. ambofaciens* (β-clamp$_{Sam}$), which is encoded by the *dnaN* gene (SAM23877_3780), was also purified following the same protocol as the one used for NucS$_{Sam}$. Its calculated molecular weight is 39882.35 Da. The gel filtration chromatogram revealed a single peak with an estimated molecular weight of approximately 97 kDa while SEC-MALS indicated a molecular weight of approximately 84 kDa. This highlighted the homodimeric nature of β-clamp$_{Sam}$ in solution and confirmed previous results obtained for β-clamp from *C. glutamicum* and *T. kodakarensis* (9,20).

NucS$_{Sam}$ mismatch-specific endonuclease activity results in DSB formation *in vitro*

Cleavage assays were performed *in vitro* to test whether purified NucS$_{Sam}$ possesses an endonuclease activity on mismatched dsDNA. The DNA substrate used in this work was a 43 bp-long dsDNA containing different combinations of mismatched base pairs at the 21st nucleotide pair. One strand of the substrate was fluorescently labeled at the 5′ end with 6FAM dye. As a control, a dsDNA substrate with no mismatch was also subjected to NucS$_{Sam}$ activity. The cleavage products generated by NucS$_{Sam}$ were analyzed qualitatively using a 10% native PAGE. No cleavage product was observed when using the control substrate. NucS$_{Sam}$ displayed cleavage activity on substrates containing G/T, T/T and G/G mismatches. The cleaved product co-migrated with a control dsDNA containing a 5′ protrusion of a five nucleotide-single-

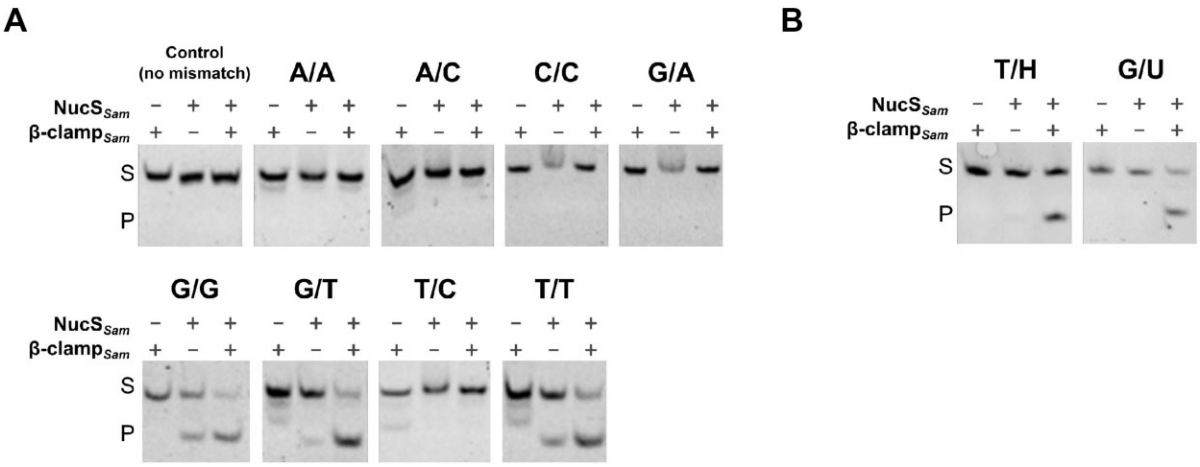

Figure 2. NucS$_{Sam}$ mismatch specific cleavage activity. (**A**) *In vitro* cleavage assays were performed with 6-FAM-labeled dsDNA substrates (43-bp, 50 nM) containing no mismatch (control) or single base-pair mismatches (A/A, A/C, C/C, G/A, G/G, G/T, T/C or T/T) or (**B**) single deaminated bases (H instead of A or U instead of C). Each substrate was incubated for 60 min at 30°C, either with 2.4 μM of NucS$_{Sam}$ or with 1.2 μM of β-clamp$_{Sam}$ or with both proteins at the above concentrations. Products were separated by 10% native PAGE. Substrates and cleavage products are indicated by 'S' and 'P' letters on the left side of the panels. The figure is representative of three experiments.

stranded DNA and expected to correspond to the product after a cleavage within the mismatch (an example is shown on Supplementary Figure S3) (20). No activity was detected with substrates containing T/C, A/A, A/C, G/A or C/C mismatches (Figure 2A shows the results of one of the three biological replicates). Notably, the addition of β-clamp$_{Sam}$ to the reaction greatly enhanced the cleavage efficiency of NucS$_{Sam}$, as evidenced by the presence of a more intense band corresponding to the cleaved substrate. The presence of β-clamp$_{Sam}$ did not alter the substrate specificity of NucS$_{Sam}$. The presence of the metallic enzymatic cofactor Mn^{2+} was always required for NucS$_{Sam}$ cleavage activity but no activity was observed with Mg^{2+} cofactor (data not shown).

Recently, an interesting study (58) showed that NucS from the euryarchaeon *Thermococcus gammatolerans* is able to cleave dsDNA containing deaminated bases such as uracil and hypoxanthine. Deamination process consists in the removal of an amino group from a molecule. In cells, deamination of DNA bases can occur spontaneously and produce mutagenic DNA lesions. Specifically, the removal of the amino groups from cytosine and adenine results in the formation of uracil (U) and hypoxanthine (H), respectively. If not repaired, these lesions can cause transition mutations since uracil pairs with adenine and hypoxanthine pairs with cytosine. We assessed whether NucS$_{Sam}$ had an endonuclease activity on dsDNA containing deaminated bases. *In vitro* cleavage tests showed that NucS$_{Sam}$ alone had no activity against G/U and T/H substrates, in contrast to the results reported by Zhang and collaborators (58) (Figure 2B). Interestingly, the activation of such mismatch-specific endonuclease activity was observed when β-clamp$_{Sam}$ was added to the reaction. These results are original as they suggest that NucS$_{Sam}$ participates in a process of DNA repair other than mismatch repair such as the base excision repair pathway.

Mutation rate is affected in *nucS*-deleted strains

To investigate the *in vivo* activity and specificity of NucS$_{Sam}$, a mutation accumulation (MA) assay was conducted. Twelve independent WT lines and three independent lines for each Δ*nucS* mutant were tracked for 60 sporulation cycles. Weekly, a single colony from each lineage was streaked onto fresh growth medium. By performing whole-genome sequencing on both parental and evolved strains, we identified the mutations that occurred throughout the MA experiment. To ensure accurate read mapping, a rigorous approach was implemented by excluding repetitive sequences from our analysis (as the 200 kb long TIR of *S. ambofaciens*). As a result, the sequence coverage for each line accounted for more than 89% of the complete *S. ambofaciens* ATCC 23877 genome. A total of 156 mutations were found in the WT lines, corresponding to an overall mutation rate of 2.84 $\times 10^{-8}$ mutation per nucleotide per sporulation cycle (Table 1). The number of generations occurring during a sporulation cycle of 7 days in *Streptomyces* was estimated to be approximately 24. Thus, the WT mutation rate would be around 1.18 $\times 10^{-9}$ per nucleotide per generation, which is comparable to that observed in *M. smegmatis* or *C. glutamicum* (19,21). The ratio of non-synonymous to synonymous mutations (dN/dS) determined by the MA assay in WT lines was 2.96 (71/24), which was not significantly different from that expected (2.54), based on the codon usage in *S. ambofaciens* ATCC 23877 strain (chi-squared test $\chi^2 = 0.4182.$, $P = 0.51$), suggesting that the selective pressure in our MA protocol was minimal.

Table 1. Total number of mutations and mutation rates determined by MA assays

Strain	Number of lineages	Average sequence coverage† (%)	Total number of mutations	Mutation rate per nucleotide per cycle ($\times 10^{-8}$)
WT	12	90.23 ± 2.49	156	2.84
Δ*nucS*	12	91.34 ± 1.78	5067	92.23
Δ*nucS-1*	3	91.34 ± 0.28	1372	100.64
Δ*nucS-2*	3	92.20 ± 0.51	1226	88.29
Δ*nucS-3*	3	92.70 ± 0.41	1319	94.52
Δ*nucS-4*	3	89.14 ± 2.30	1150	85.39

†The sequence coverage corresponds to the percentage of the reference genome of *S. ambofaciens* (ATCC 23877: 8303940 bp) analyzed for mutation call between evolved lines and their parental strains.

Table 2. Spectrum of base pair substitutions (BPSs) and indels

	WT			Δ*nucS*		
	Number	Percentage (%)	Mutation rate per nucleotide per cycle ($\times 10^{-8}$)	Number	Percentage (%)	Mutation rate per nucleotide per cycle ($\times 10^{-8}$)
BPSs	147	100	2.67	5048	100	91.88
Transitions	73	49.66	1.33	4908	97.23	89.33
A:T > G:C	32	21.77	0.58	2986	59.15	54.35
G:C > A:T	41	27.89	0.75	1922	38.07	34.98
Transversions	74	50.34	1.35	140	2.77	2.55
A:T > T:A	5	3.55	0.09	12	0.24	0.22
A:T > C:G	6	3.55	0.11	20	0.40	0.36
G:C > T:A	18	11.35	0.33	34	0.67	0.62
G:C > C:G	45	31.21	0.82	74	1.47	1.35
Indels	9	100	0.16	19	100	0.35
Insertions	3	33.33	0.05	9	47.37	0.16
Deletions	6	66.67	0.11	10	52.63	0.18

Overall, the 12 Δ*nucS* lines exhibited a total of 5067 mutations (Table 1). The 3 evolved lines derived from each Δ*nucS* independent mutant exhibited an accumulation of mutations ranging from 1150 to 1372 (Table 1). The deletion of *nucS* resulted in a significant 32-fold average increase in the mutation rate per nucleotide per cycle, with rates of 2.8×10^{-8} for the WT and an average of 9.2×10^{-7} for the four Δ*nucS* mutants. The ratio of dN/dS mutations in Δ*nucS* lines was 3.13 (3280/1048), which was significantly different from that expected of 2.54 (chi-squared test $P < 10^{-5}$) but not significantly different from the d*N*/d*S* obtained in WT lines (chi-squared test $P = 0.11$). Thus, the results obtained with the mutants appear to be close to, but slightly above, the expected result for an unbiased distribution of non-synonymous and synonymous mutations.

Mutational spectrum is shifted upon NucS$_{Sam}$ loss

The mutational profiles and rates of base pair substitutions (BPSs) in *S. ambofaciens* WT and Δ*nucS* lines are shown in Table 2. In the WT MA lines, a total of 147 BPSs was identified, corresponding to a rate of 2.67×10^{-8} BPS per nucleotide per cycle. This rate is consistent with the previously reported BPS rate in *S. coelicolor*, which was about 1.50×10^{-8} BPS per nucleotide per cycle (59). Furthermore, in the 12 Δ*nucS* lines, a total of 5048 BPSs was detected, resulting in a BPS mutation rate of 9.19×10^{-7} per nucleotide per cycle. This substantial increase represents a remarkable 34-fold difference compared to the WT MA lines. Additionally, our analysis unveiled the presence of 9 indels in the WT lines, ranging from 1 to 4 bp in length, while we detected 19 indels (of 1–2 bp) in the absence of NucS$_{Sam}$. Therefore, the loss of NucS$_{Sam}$ did not considerably affect the rate of indels (5×10^{-10} versus 1.6×10^{-9} for WT and *ΔnucS*, respectively).

Regarding the BPSs in the WT, the transition/transversion ratio was 1.01 (49.7% versus 50.3% respectively). The most prevalent mutation type was G:C > C:G, accounting for 31.2% of total BPSs. Of note, G:C > A:T and A:T > G:C transitions were the second and third most frequent mutation types (27.9% and 21.8% of the BPSs, respectively). The inactivation of NucS$_{Sam}$ caused a significant bias in the spectrum towards transitions, which accounted for 97.2% of the substitutions whereas only 2.8% of the BPSs were transversions. Consequently, this resulted in a high transition/transversion ratio of 36.1, which was 36-fold higher than that of the WT lines. In addition, Δ*nucS* lines exhibited a remarkable 67-fold increase in the transition mutation rate, while the transversion mutation rate underwent a modest 2-fold increase. Overall, the rates of mutation for all substitutions were higher in *nucS*-deleted lines compared to WT (Figure 3), but it is noteworthy that the mutation rate of the A:T > G:C and G:C > A:T substitutions increased strikingly in the mutant with 94-fold and 47-fold increases, respectively. Altogether, the deletion of *nucS* resulted in a significant shift in the BPS bias, particularly towards A:T > G:C transitions, which accounted to 59.2% of all observed BPSs.

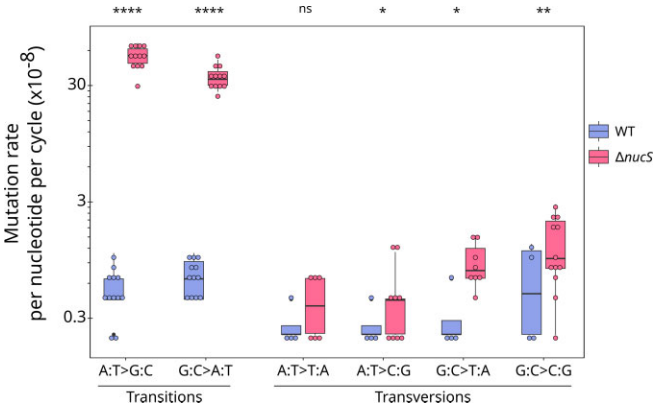

Figure 3. Transition and transversion rates in WT and Δ*nucS* lines. The top of each boxplot indicates 75% percentile, the bottom 25% percentile, and the thick bar inside the box is the median. The minimum and maximum values are shown by the whiskers. Individual data values for each line are represented by circles. Statistical significance levels are denoted as follows: *$P < 0.05$, **$P < 0.01$, ****$P < 0.0001$ and ns stands for non-significant (Wilcoxon rank sum test).

Transition frequency increases towards the extremities of the chromosome

The *S. ambofaciens* chromosome replicates from a centrally located origin of replication towards its ends, defining two replichores of equivalent size. To assess the distribution of transitions along the *S. ambofaciens* chromosome in the twelve evolved lines, the number of transitions was counted within a sliding non-overlapping 100 kb window, starting from *dnaA* gene (at position 4021374, approximately corre-

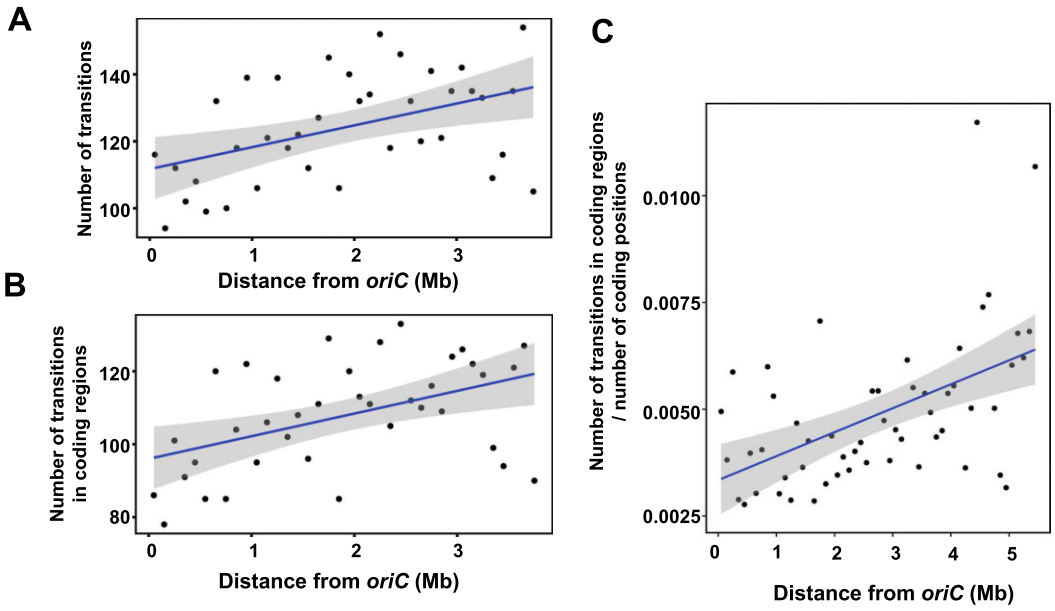

Figure 4. Transition distribution along *Streptomyces* chromosome. (A and B) Transitions along the chromosome of the 12 *S. ambofaciens* evolved Δ*nucS* lines were counted within a non-overlapping 100 kb window, starting from *dnaA* gene (located in the middle of the chromosome at position 4021374 and approximately corresponding to the origin of replication, *oriC*) and sliding towards the chromosome extremities. The number of transitions in windows of the right replichore was added to the number of transitions of windows at the same distance of *dnaA* in the left replichore. The sum of total transitions (**A**) or the sum of transitions restricted to the coding sequences (**B**) was represented as a function of the distance from *dnaA*. Significant positive correlations were observed between the genomic position and the transition count (Pearson's correlation coefficient $r = 0.457$, $P = 0.004$) or the number of transitions within the coding sequences (Pearson's correlation coefficient $r = 0468$, $P = 0003$). (**C**) Transition distribution was estimated along the chromosome of environmental strain RLB1-8 compared to the environmental strain RLB3-17. As above, transitions within coding regions, on orthologous pairs of genes (BLASTp reciprocal best hits with at least 40% identity, 70% coverage, and an *E*-value lower than 1e-10), were counted within a non-overlapping 100 kb window starting from *dnaA* gene (corresponding to *oriC*, approximately at position 6204383 in RLB1-8). The number of transitions in windows of the right replichore was added to the number of transitions of windows at the same distance of *dnaA* in the left replichore and the sum was normalized to the total number of coding positions of the window. A significant positive correlation was observed between the transition count and the genomic position (Kendall rank correlation test $r = 0.38$, $P = 0{,}00005$).

sponding to the replication origin *oriC*), extending towards the left or the right end of the chromosome and plotted as a function of the distance from *dnaA* (Figure 4A). A significant positive correlation was observed between the number of transitions and the genomic position for Δ*nucS* lines (Pearson's correlation coefficient $r = 0.457$, $P = 0.004$). This suggests that in the absence of NucS, transitions have a crescent-shaped distribution with a minimum at the replication origin of the chromosome. There was no significant correlation for the transition distribution in the chromosomes of the twelve WT lines, probably because the sample size is too small (73 transitions in total). Since 97.3% of all the BPSs are transitions in Δ*nucS* lines, an increase in the BPS number towards the extremities was also observed (Supplementary Figure S4A). When only considering the transitions in coding regions (Figure 4B), the same increasing trend is again noticed (Pearson's correlation coefficient $r = 0468$, $P = 0003$). As a low occurrence of mutations in the central part of the chromosome could be due to negative selection of mutations in essential genes, non-synonymous and synonymous mutations within coding sequences were counted along the chromosome of Δ*nucS* lines and plotted as above. Non-synonymous mutation frequency (Supplementary Figure S4B) increased significantly towards the arm ends (Pearson's correlation coefficient $r = 0.499$, $P = 0.001$), but no trend was observed for synonymous mutations (Supplementary Figure S4C). However, the positive correlation found between the non-synonymous mutation number and the genomic position was lost when the non-synonymous mutation number was plotted against the number of synonymous mutations for each position (Supplementary Figure S4D). Indeed, the ratio between non-synonymous and synonymous mutations is homogeneous along the genome, suggesting that there is no clear selection difference depending on the genomic position.

As BPS accumulation is low in the WT evolved lines, we decided to estimate the accumulation of transitions by comparing WT genomes of strains that have been diverging for much longer than 60 sporulation cycles. Therefore, the genomes of *Streptomyces* environmental strains RLB1-8 and RLB3-17 (51) sharing an average nucleotide identity (ANI) of 99.19% were compared in terms of SNP distribution. Orthologs were defined by pairwise comparison of both strain genomes and detection of transitions was first specifically done in orthologous pairs. As above, the number of transitions was counted within a sliding non-overlapping 100 kb window, starting from *oriC* (estimated at position 6204383 by the *dnaA* gene location in RLB1-8 genome, which was used as the reference), extending towards the left or right end of the chromosome. The sum of equidistant windows on the left and the right replichores was normalized to the total number of coding positions included in the windows (to consider the possible differential density of orthologous genes along the chromosome) and plotted as a function of the distance from *oriC*. As shown in Figure 4C, a clear increase of transition number in orthologous genes is observed when the distance from the origin of replication increases (Kendall rank correlation test $r = 0{,}38$

$P = 0{,}00005$). When considering the whole genome and not only the coding regions, the transitions are also clearly more frequent when moving away from *oriC* (Kendall rank correlation test $r = 0{,}33$ $P = 0.00045$) (Supplementary Figure S5). The comparison of genomes of other conspecific strains isolated from the same soil grain showed a similar increasing trend towards the chromosome termini (data not shown). Altogether, these results indicate that a short time evolutionary scale is sufficient to observe transition accumulation with a crescent-shaped distribution along the chromosome of WT strains possessing a functional non-canonical MMR.

Occurrence of BPSs has a strong DNA-strand bias

When considering the 5′ to 3′ nucleotide sequence ('top strand') of *S. ambofaciens* chromosome, the left replichore (starting at the left end to the *oriC* position) corresponds to the lagging strand while the right replichore (starting at *oriC* to the right end) corresponds to the leading strand. The A:T > G:C transitions occur when C is mispaired with template A or G is mispaired with template T. Considering one strand, A:T > G:C transitions are either A > G or T > C, and our results in Δ*nucS* evolved lines (Supplementary Table S3) showed that in the leading strand (right replichore), A > G substitutions were three times more frequent than T > C substitutions (1150 versus 412, respectively). This bias was reversed in the lagging strand (left replichore) where mispaired Ts occurred more often than mispaired As (1031 Ts versus 393 As). This means that during replication, A:T > G:C transitions are more likely to originate from a C in the lagging strand mispaired to template A and a G in the leading strand mispaired to a template T than the contrary. Likewise, a similar strand bias was found for G:C > A:T transitions with more C > T than G > A substitutions in the right replichore (715 versus 274, respectively); the reversed trend was observed in the left replichore (234 versus 699, respectively). Thus G:C > A:T transitions are more likely to originate from a A in the lagging strand mispaired to template C and a T in the leading strand mispaired to a template G than the contrary. This transition strand bias is consistent with the observations made in MMR defective *E. coli* (4), *M. smegmatis* (19), and also C. *glutamicum* (21). Since this finding was made in the mutant lines lacking a functional MMR, and since $NucS_{Sam}$ was able to target G/T but not A/C mismatches *in vitro*, it is possible that transitions arise more frequently from a G mispaired to a T on the lagging strand template than a T on the leading strand template, which would indicate a nucleotide misincorporation bias by the DNA polymerase, as suggested in *E. coli* (60). No strand bias could be observed in the WT evolved lines, because the mutation rate is too low. Therefore, further investigation is needed to clarify a possible strand-specific activity of the non-canonical MMR.

Discussion

Streptomyces species, like the majority of actinobacteria, do not possess the signature proteins of the canonical MMR pathway, MutSL. The discovery of NucS in archaea as part of an alternative MMR pathway prompted further investigation. NucS is not only found in many archaea but also widely conserved among most actinobacteria (9,18). In our analysis, we found that $NucS_{Sam}$ is highly conserved within the *Streptomyces* genus, establishing *nucS* as a core gene in these bacteria. *S. ambofaciens* Δ*nucS* mutant displayed a hypermutable phenotype characterized by the appearance of sectored colonies. A sector on a colony (with a radial growth) is a visible different hyphal phenotype resulting from a mutation that occurred during the colony growth. The frequency of sectors is therefore a visual indication of mutation rate. The increased emergence of rifampicin-resistant colonies in the progeny of Δ*nucS* mutant also indicated a significantly increased spontaneous mutation rate. These results are consistent with previous studies conducted in other actinobacterial species, and provide additional evidence for the role of NucS in genome maintenance (18,20,21). Our biochemical study demonstrated that $NucS_{Sam}$ targets G/T, T/T and G/G dsDNA substrates by cleaving both strands, resulting thus in a DSB. This cleavage mechanism and preference are in accordance with those described in archaeal species and in *C. glutamicum* (9,20,21). The Mn^{2+} enzymatic cofactor was required for $NucS_{Sam}$ activity, in the presence or absence of β-$clamp_{Sam}$. However, no cleavage activity was observed with Mg^{2+} for $NucS_{Sam}$. This differs from NucS from *T. kodakarensis* and *C. glutamicum* which use both Mn^{2+} and Mg^{2+} (9,20,21). Such activity has not yet been shown in *Mycobacterium* species, and one of the suggested hypotheses was the need for other partners (18). Indeed, the endonuclease activity of $NucS_{Sam}$ was significantly enhanced by the presence of the β-clamp, a crucial protein involved in DNA replication. This interaction with β-clamp is essential for efficient mutation avoidance and genome stability in *C. glutamicum* (20,21). It has been hypothesized that the β-clamp could induce a conformational change that favors DNA binding or induce the catalytic step (17) but most importantly, it could tether the MMR enzyme to the replication zone where mismatches occur (21). The coupling of canonical MMR to the β-clamp has also been demonstrated as the interaction of MutS and MutL with β-clamp is necessary for a functional MMR in *E. coli* and in *B. subtilis* (12,61,62).

Our biochemical study also revealed an additional endonuclease activity of $NucS_{Sam}$ on deaminated substrates such as G/U and T/H mismatches. Interestingly, this activity was only observed in the presence of β-clamp. This suggests that $NucS_{Sam}$, together with β-clamp, plays a role in the repair of DNA lesions resulting from deamination similar to the base excision repair (BER) pathway. Conversion of cytosine to uracil leads to G:C > A:T base pair mutation in the subsequent DNA replication. Uracil-DNA glycosylase (UDG) is a key enzyme that cleaves the N-glycosidic bond thereby initiating the BER pathway. It has been shown that UDG genes are highly conserved across *Streptomyces* genus and that the deletion of these genes is not lethal in *Streptomyces lividans* (63), nor in *E. coli* (64). Nevertheless, it is conceivable that, in addition to UDGs, $NucS_{Sam}$ may play a significant role in the BER-like pathway in *Streptomyces*. This hypothesis is supported by structural and biochemical investigations of NucS from the hyperthermophilic archaeon *T. gammatolerans*, which is thought to be involved in an alternative pathway for the repair of deaminated bases (58). The study has highlighted that the ends of cleaved dsDNA products could be utilized by homologous recombination proteins. However, the involvement of PCNA was not investigated in this study. Our results suggest that the activity of $NucS_{Sam}$ on deaminated bases is coupled to replication, as it requires the presence of β-clamp. A possibility is that $NucS_{Sam}$ plays a role in a mechanism similar to pre-replicative BER. Pre-replicative BER, mainly described in eukaryotes, is thought to target and repair base le-

sions on DNA template in front of the replication fork and this function has been linked to the DNA-glycosylase NEIL1 and to PCNA in human cells (65). Interestingly, *M. tuberculosis* Nei2, a BER glycosylase that removes oxidized base lesions from ssDNA and replication fork-mimicking substrates, has recently been shown to interact with β-clamp, which enhances its activity (66,67). $NucS_{Sam}$, through its interaction with $\beta\text{-clamp}_{Sam}$, could have a similar role in targeting deaminated bases in front of the replication forks. However, it remains unclear whether and how $NucS_{Sam}$ targets deaminated base sites that arise spontaneously independently of replication, for example during oxidative stress.

A significant transition-biased spectrum was observed in Δ*nucS* strains through MA assays. This is in line with previous works in actinobacteria and archaea (19,21,68). Such transition shift is a well-established hallmark of MMR deficiency as observed in organisms bearing a canonical MMR such as *E. coli* (4). It is indeed known that transition mispairs are less efficiently proofread than transversions, making them specific targets of MMR machineries (69). It is important to point out that Δ*nucS* lines accumulate more A:T > G:C than G:C > A:T transitions whereas the opposite is observed in WT lines. Thus, the non-canonical MMR could prevent the accumulation of GCs in *Streptomyces* genomes, which already have a high GC content, as suggested for GC-rich mycobacterial genomes (19), and also with opposite observations in *E. coli* genome (50% GC) (4). A very interesting result is the correlation that can be made with our *in vivo* and *in vitro* findings. Indeed, *in vitro* activities revealed that the G/T mismatch is clearly one of the preferred substrates of $NucS_{Sam}$, whereas no cleavage activity on A/C mispair could be detected. Such striking preference was also observed with NucS from *T. kodakarensis* (9) and *C. glutamicum* (20,21). Furthermore, recent oligonucleotide recombination experiments in *M. smegmatis* yet to be published (70) revealed that *in vivo* NucS would only correct G/T but not A/C mismatches in this species. In this case, transition events in MMR-deficient Δ*nucS* lines are due to uncorrected G/T mismatches. For example, during replication, a G > A transition can arise from a mispaired G/T or a mispaired C/A (Figure 5, upper panel). Since NucS only targets G/T mismatches, the increase of G > A transition mutation in the absence of NucS is due to accumulation of G/Ts (Figure 5, lower panel), and this is also true for C > T, A > G and T > C transitions. Therefore, the drastic transition accumulation in *Streptomyces* Δ*nucS* lines reflects the frequency of G/T mismatch occurrence while the negligible frequency of uncorrected A/C mispair events can be estimated by the residual transition accumulation in genomes of WT lines possessing a functional non-canonical MMR. These results enable to discriminate which transition mispairing is the most frequent during incorporation of nucleotides by DNA polymerase. The replication complex is thereby prone to generate far more G/T than C/A mismatches. Our results, supported by MA and biochemical studies on *C. glutamicum* (20,21), highlight a remarkable *in vivo* property of the DNA polymerase. The hypothesis that G/T mismatches are much more likely to occur *in vivo* has previously been proposed for canonical MMR-bearing bacteria, since MutS protein preferentially binds G/T over A/C (71). MA assays in yeast showed that G pairing with T is the most common mispair generated by DNA polymerase (72). Many studies on DNA polymerase fidelity have been performed *in vitro*, and recently a high throughput analysis based on next-generation

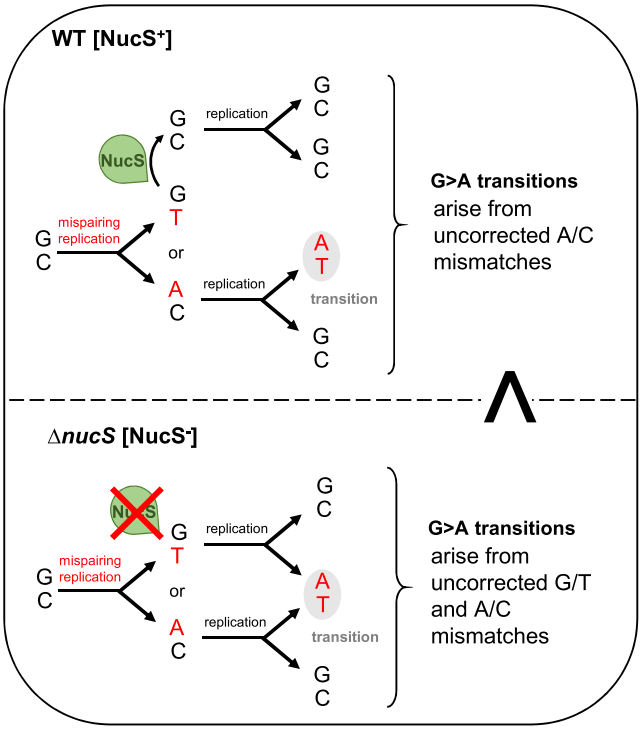

Figure 5. Implication of NucS mismatch preference in transition events during replication. The diagram illustrates the events leading to the base substitution of a G into an A, which is one of the four transitions that can occur on one strand during replication (the others being A > G, C > T and T > C). The sequence of events is described in WT bacteria possessing a functional non-canonical MMR (NucS endonuclease is active) and in a Δ*nucS* strain (lacking NucS-dependent MMR). Mutated Δ*nucS* lines accumulated far more G > A transitions than WT lines (shown with a superscript >).

sequencing showed general DNA polymerase preference for dGTP and dTTP misincorporation at T and G bases (73). This preference can be explained by tautomer occurrence and stability, and spatial constraints in the polymerase active site during catalysis of the phosphodiester bond (74–78). The DNA bases exist as tautomers (interchangeable pairs of isomers), and A/T and G/C base pairs contain each base in its predominant tautomeric form. Watson and Crick (79) proposed that if nucleotide bases adopted their energetically less favorable tautomeric forms, mismatches could arise in a Watson–Crick (WC)-like geometry and consequently lead to spontaneous mutations. However, it is only in the last decade that this 70-year-old model has been experimentally validated, and, in particular, G/T tautomers were demonstrated to exist during DNA polymerization and to have a role in base pair mis-incorporation and transition occurrence (80). Altogether, these data underline the propensity of DNA polymerases to produce G/T mispairs and our *in vivo* results together with observations in *C. glutamicum* (20,21) demonstrate that these G/T mismatches are specifically eliminated by a NucS-dependent MMR mechanism, which has evolved to correct these frequent transition mismatches in cells.

Another remarkable observation is that accumulation of mutations in evolved Δ*nucS* lines correlates with the distance to the origin of replication. It is noteworthy that the frequency of transitions, which represent the vast majority of mutations in the mutant, follows the same trend. This crescent-shaped

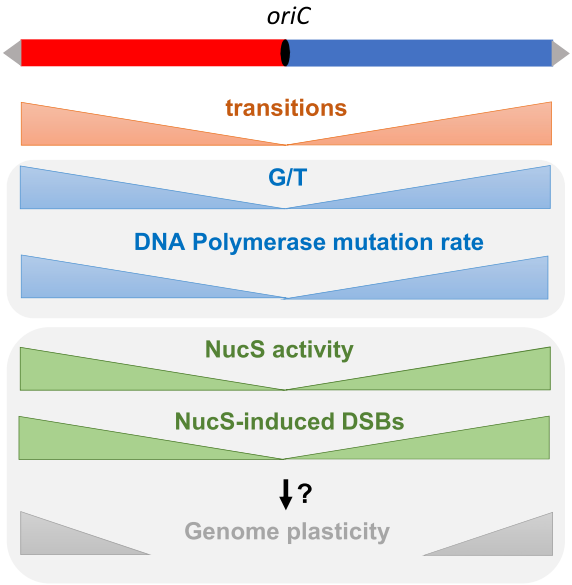

Figure 6. DNA polymerase mutation rate and non-canonical MMR activity along the chromosome during replication in *Streptomyces*. Red and blue boxes represent left and right replichores of the chromosome. Grey arrows represent the terminal inverted repeats at each chromosome extremity. In MMR defective (Δ*nucS*) lines, the transition density increases towards the extremities of the chromosome. Because $NucS_{Sam}$ cleaves G/T but not A/C mismatches *in vitro*, this transition trend suggests an increase of G/T mispairing and an increase in DNA polymerase mutation rate towards the extremities (in blue). This observed mutation profile also suggests that in MMR proficient (WT) lines, NucS activity increases with the distance of the replication origin, and thus NucS-induced DSBs are more frequent towards the extremities of the chromosome (in green). Assuming that these DSBs are repaired by recombination, this profile is in accordance with the recombination gradient driving the genome plasticity described in *Streptomyces* (illustrated in grey).

BPS distribution in the absence of a functional MMR reflects a variable mutation rate of DNA polymerase (due to variable accuracy or an imbalance in the nucleotide pools) and/or a differential selection along the chromosome. It is known that core genes are located in the central compartment of the chromosome in *Streptomyces* (29) and, although there is no data on the distribution of essential genes, it can be argued that most essential genes are among the core genes, so it is likely that some mutations in the central region of the chromosome are counter-selected. A commonly used way of assessing selection bias is the ratio of non-synonymous to synonymous mutations, assuming that synonymous mutations are relatively neutral. Our results showed that there was no correlation between the d*N*/d*S* ratio and the genomic position in the evolved Δ*nucS* lines. Therefore, the BPS distribution in the absence of a functional MMR reflects the distribution of mismatches that occur during replication and suggests an increasing mutation rate of the DNA polymerase towards the extremities (Figure 6). Given the propensity of DNA polymerase to generate G/T mismatches (as discussed above), this implies that G/T mispairs accumulate with the distance from the replication origin, a finding that, to our knowledge, has never been documented for bacterial linear chromosomes. Furthermore, our results of differential mutation rate along the chromosome suggest that different areas of the genome evolve at different rates in *Streptomyces*, implying that the genes located closer to the replication origin are less prone to evolution than those closer to the termini, which is consistent with the compartmentalization of *Streptomyces* chromosome (29). In WT evolved lines, the low total number of mutations prevented us from building a robust statistical model for transition distribution. However, the comparison of genomes of two close *Streptomyces* individuals isolated from a soil grain and deriving from a recent common ancestor revealed that the transition rate increases significantly with the distance from the origin. This finding suggests that this short time evolutionary scale is long enough to observe that transitions in WT environmental strains tend to accumulate in the extremities of the chromosome, where transition mismatches are more likely to occur and/or escape proofreading and MMR activities. Pioneering studies on *E. coli* and *Salmonella typhimurium* genomes indicated that genes located further from the replication origin have higher mutation rates than those closer to the origin (81,82), and some studies suggest that it is the proximity to the fragile replication termination sites that is responsible for this phenomena (83,84). In the last decade, MA studies on lines lacking MMR in *E. coli* or *Bacillus subtilis* (85,86) and in *Vibrio* and *Pseudomonas* species (87) revealed a more precise wave-like pattern that is symmetrical about the replication origin. Such wave-like pattern of mutation distribution was not visible in the genome of evolved Δ*nucS* lines, either because the total number of mutations in this study is not high enough to build such a model, or because the *Streptomyces* linear chromosome has a different tridimensional structure (see below). In *E. coli*, it has been observed that intrinsic errors by the DNA polymerase occur more frequently near the replication origin, but also that error correction by the proofreading activity of the DNA polymerase or canonical MMR is more effective close to the *oriC* region. More importantly, it has been hypothesized that DNA replication becomes inaccurate in regions of high superhelical density and that nucleoid-associated protein (NAP) binding increases mutability by impeding DNA repair and/or interfering with DNA polymerase processivity during replication (84,86,88). *Streptomyces* NAPs are numerous and their binding along the chromosome is temporally and spatially variable throughout the bacterial life cycle (89–91) such that the association between NAPs and mutation density is complicated. An interesting example is the HU family-protein HupS which participates in chromosomal spatial rearrangement and compaction at the onset of sporulation in *Streptomyces venezuelae* (90). Increased binding of HupS to the subterminal regions organize them into a closed structure, that might be prone to a higher mutation rate.

Although several studies revealed a cleavage activity of NucS on mismatched DNA and the generation of a DSB *in vitro*, such activity has not been demonstrated *in vivo* and further investigations are needed to elucidate this particularity of the non-canonical MMR. The mechanism by which NucS-mediated DSBs would be repaired remains elusive. The involvement of homologous recombination to process the unwanted DSB is the most obvious hypothesis and would allow a mismatch repair without strand discrimination. The recruitment of homologous recombination to DNA damage could be achieved *via* the replication clamp which is a known platform that recruits numerous DNA-processing enzymes including DNA repair enzymes (92). Besides, unlike most bacteria, *Streptomyces* species also have the ability to repair DSBs by illegitimate recombination pathway. Our previous work has demonstrated the existence of a functional NHEJ pathway in

Streptomyces (37). Hence, NucS-dependent DSBs may also be repaired by NHEJ in *Streptomyces*. Very recently, a preprint manuscript (70) suggested that mycobacterial NucS participates in a MMR reaction involving short patch repair confined within 5–6 bp of the mispaired nucleotides, which appears to be mechanistically distinct from repair by homologous recombination or NHEJ DSB repair mechanisms. A similar study in *M. smegmatis*, not approved by peer review yet, has also shown that a NucS-promoted DSB is processed by a 5′–3′ exonuclease, but is independent of both RecA, RadA and NHEJ functions Ku and LigD (93).

The high level of genetic instability observed in the *Streptomyces* genus is one of its most intriguing features and DSB repair is thought to be the main driver of this instability (35). The increasing occurrence of mismatches towards the ends of the chromosome suggests that NucS activity is more required further from the origin and consequently that more DSBs occur in the subtelomeric regions (Figure 6). Several studies have pointed to the existence of a recombination gradient towards the chromosomal arms highlighting the compartmentalization of the *Streptomyces* genome (29,51). Our results support an increase of DSBs towards the ends of the chromosome, contributing to increased recombination events in the extremities and thus to the unique organization of the *Streptomyces* chromosome. Yet, how the NucS-dependent DSBs are repaired remains to be elucidated. Additional aspects such as differential efficiency of DSB repair along the chromosome as well as the involvement of the spatial conformation of the chromosome (94) or the role of chromatin-organizing proteins (90) need to be considered to gain a comprehensive understanding of *Streptomyces* genome dynamics.

Data availability

The sequencing data underlying this article have been deposited with links to BioProject accession number PRJNA1047308 in the NCBI BioProject database (https://www.ncbi.nlm.nih.gov/bioproject/).

Supplementary data

Supplementary Data are available at NAR Online.

Acknowledgements

This work benefited from the ASIA platform (Université de Lorraine-INRAE; https://a2f.univ-lorraine.fr/en/asia-2/). The authors would like to acknowledge Tiphaine Dhalleine (IAM, Université de Lorraine, INRAE) for the technical expertise with SEC-MALS analyses.

Funding

French National Research Agency program MM-RDNABREAK [ANR-22-CE12-0042-02]. Funding for open access charge: French Agency for Research [MM-RDNABREAK ANR-22-CE12-0042-02].

Conflict of interest statement

None declared.

References

1. Ganai,R.A. and Johansson,E. (2016) DNA replication—a matter of fidelity. *Mol. Cell*, **62**, 745–755.
2. Li,G.-M. (2008) Mechanisms and functions of DNA mismatch repair. *Cell Res.*, **18**, 85–98.
3. Putnam,C.D. (2021) Strand discrimination in DNA mismatch repair. *DNA Repair (Amst.)*, **105**, 103161.
4. Lee,H., Popodi,E., Tang,H. and Foster,P.L. (2012) Rate and molecular spectrum of spontaneous mutations in the bacterium *Escherichia coli* as determined by whole-genome sequencing. *Proc. Natl. Acad. Sci. U.S.A.*, **109**, E2774–E2783.
5. Sachadyn,P. (2010) Conservation and diversity of MutS proteins. *Mutat. Res./Fundam. Mol. Mech. Mutagen.*, **694**, 20–30.
6. Busch,C.R. and DiRuggiero,J. (2010) MutS and MutL are dispensable for maintenance of the genomic mutation rate in the halophilic archaeon *Halobacterium salinarum* NRC-1. *PLoS One*, **5**, e9045.
7. Kucukyildirim,S., Long,H., Sung,W., Miller,S.F., Doak,T.G. and Lynch,M. (2016) The rate and spectrum of spontaneous mutations in *Mycobacterium smegmatis*, a bacterium naturally devoid of the postreplicative mismatch repair pathway. *G3*, **6**, 2157–2163.
8. Ren,B., Kühn,J., Meslet-Cladiere,L., Briffotaux,J., Norais,C., Lavigne,R., Flament,D., Ladenstein,R. and Myllykallio,H. (2009) Structure and function of a novel endonuclease acting on branched DNA substrates. *EMBO J.*, **28**, 2479–2489.
9. Ishino,S., Nishi,Y., Oda,S., Uemori,T., Sagara,T., Takatsu,N., Yamagami,T., Shirai,T. and Ishino,Y. (2016) Identification of a mismatch-specific endonuclease in hyperthermophilic Archaea. *Nucleic Acids Res.*, **44**, 2977–2986.
10. Maga,G. and Hubscher,U. (2003) Proliferating cell nuclear antigen (PCNA): a dancer with many partners. *J. Cell Sci.*, **116**, 3051–3060.
11. Moldovan,G.-L., Pfander,B. and Jentsch,S. (2007) PCNA, the maestro of the replication fork. *Cell*, **129**, 665–679.
12. Saro,F.J.L.d., Marinus,M.G., Modrich,P. and O'Donnell,M. (2006) The β sliding clamp binds to multiple sites within MutL and MutS. *J. Biol. Chem.*, **281**, 14340–14349.
13. Pluciennik,A., Burdett,V., Lukianova,O., O'Donnell,M. and Modrich,P. (2009) Involvement of the β clamp in methyl-directed mismatch repair *in Vitro*. *J. Biol. Chem.*, **284**, 32782–32791.
14. Meslet-Cladiére,L., Norais,C., Kuhn,J., Briffotaux,J., Sloostra,J.W., Ferrari,E., Hübscher,U., Flament,D. and Myllykallio,H. (2007) A novel proteomic approach identifies new interaction partners for proliferating cell nuclear antigen. *J. Mol. Biol.*, **372**, 1137–1148.
15. Creze,C., Ligabue,A., Laurent,S., Lestini,R., Laptenok,S.P., Khun,J., Vos,M.H., Czjzek,M., Myllykallio,H. and Flament,D. (2012) Modulation of the *Pyrococcus abyssi* NucS endonuclease activity by replication clamp at functional and structural levels. *J. Biol. Chem.*, **287**, 15648–15660.
16. Dalrymple,B.P., Kongsuwan,K., Wijffels,G., Dixon,N.E. and Jennings,P.A. (2001) A universal protein–protein interaction motif in the eubacterial DNA replication and repair systems. *Proc. Natl. Acad. Sci.*, **98**, 11627–11632.
17. Nakae,S., Hijikata,A., Tsuji,T., Yonezawa,K., Kouyama,K., Mayanagi,K., Ishino,S., Ishino,Y. and Shirai,T. (2016) Structure of the EndoMS-DNA complex as mismatch restriction endonuclease. *Structure*, **24**, 1960–1971.
18. Castañeda-García,A., Prieto,A.I., Rodríguez-Beltrán,J., Alonso,N., Cantillon,D., Costas,C., Pérez-Lago,L., Zegeye,E.D., Herranz,M., Plociński,P., *et al.* (2017) A non-canonical mismatch repair pathway in prokaryotes. *Nat. Commun.*, **8**, 14246.
19. Castañeda-García,A., Martín-Blecua,I., Cebrián-Sastre,E., Chiner-Oms,A., Torres-Puente,M., Comas,I. and Blázquez,J. (2020) Specificity and mutagenesis bias of the mycobacterial alternative mismatch repair analyzed by mutation accumulation studies. *Sci. Adv.*, **6**, eaay4453.
20. Ishino,S., Skouloubris,S., Kudo,H., l'Hermitte-Stead,C., Es-Sadik,A., Lambry,J.-C., Ishino,Y. and Myllykallio,H. (2018) Activation of the mismatch-specific endonuclease EndoMS/NucS

by the replication clamp is required for high fidelity DNA replication. *Nucleic Acids Res.*, **46**, 6206–6217.
21. Takemoto,N., Numata,I., Su'etsugu,M. and Miyoshi-Akiyama,T. (2018) Bacterial EndoMS/NucS acts as a clamp-mediated mismatch endonuclease to prevent asymmetric accumulation of replication errors. *Nucleic Acids Res.*, **46**, 6152–6165.
22. Fressatti Cardoso,R., Martín-Blecua,I., Pietrowski Baldin,V., Meneguello,J.E., Valverde,J.R., Blázquez,J. and Castañeda-García,A. (2022) Noncanonical mismatch repair protein NucS modulates the emergence of antibiotic resistance in *Mycobacterium abscessus*. *Microbiol. Spectr.*, **10**, e02228-22.
23. Iliakis,G. (1991) The role of DNA double strand breaks in ionizing radiation-induced killing of eukaryotic cells. *Bioessays*, **13**, 641–648.
24. Kuzminov,A. (1999) Recombinational repair of DNA damage in *Escherichia coli* and bacteriophage lambda. *Microbiol. Mol. Biol. Rev.*, **63**, 751–813.
25. Glickman,M.S. (2014) Double-strand DNA break repair in mycobacteria. *Microbiol. Spectr.*, **2**, https://doi.org/10.1128/microbiolspec.MGM2-0024-2013.
26. Bertrand,C., Thibessard,A., Bruand,C., Lecointe,F. and Leblond,P. (2019) Bacterial NHEJ: a never ending story. *Mol. Microbiol.*, **111**, 1139–1151.
27. Barka,E.A., Vatsa,P., Sanchez,L., Gaveau-Vaillant,N., Jacquard,C., Meier-Kolthoff,J.P., Klenk,H.-P., Clément,C., Ouhdouch,Y. and van Wezel,G.P. (2016) Taxonomy, physiology, and natural products of actinobacteria. *Microbiol. Mol. Biol. Rev.*, **80**, 1–43.
28. Ikeda,H., Ishikawa,J., Hanamoto,A., Shinose,M., Kikuchi,H., Shiba,T., Sakaki,Y., Hattori,M. and Ōmura,S. (2003) Complete genome sequence and comparative analysis of the industrial microorganism *Streptomyces avermitilis*. *Nat. Biotechnol.*, **21**, 526–531.
29. Lorenzi,J.-N., Lespinet,O., Leblond,P. and Thibessard,A. (2021) Subtelomeres are fast-evolving regions of the *Streptomyces* linear chromosome. *Microb. Genom.*, **7**, 000525.
30. Choulet,F., Aigle,B., Gallois,A., Mangenot,S., Gerbaud,C., Truong,C., Francou,F.-X., Fourrier,C., Guérineau,M., Decaris,B., *et al.* (2006) Evolution of the terminal regions of the *Streptomyces* linear chromosome. *Mol. Biol. Evol.*, **23**, 2361–2369.
31. Leblond,P., Demuyter,P., Moutier,L., Laakel,M., Decaris,B. and Simonet,J.M. (1989) Hypervariability, a new phenomenon of genetic instability, related to DNA amplification in *Streptomyces ambofaciens*. *J. Bacteriol.*, **171**, 419–423.
32. Leblond,P., Demuyter,P., Simonet,J.M. and Decaris,B. (1990) Genetic instability and hypervariability in *Streptomyces ambofaciens*: towards an understanding of a mechanism of genome plasticity. *Mol. Microbiol.*, **4**, 707–714.
33. Birch,A., Häusler,A. and Hütter,R. (1990) Genome rearrangement and genetic instability in *Streptomyces* spp. *J. Bacteriol.*, **172**, 4138–4142.
34. Fischer,G., Wenner,T., Decaris,B. and Leblond,P. (1998) Chromosomal arm replacement generates a high level of intraspecific polymorphism in the terminal inverted repeats of the linear chromosomal DNA of *Streptomyces ambofaciens*. *Proc. Natl. Acad. Sci. U.S.A.*, **95**, 14296–14301.
35. Hoff,G., Bertrand,C., Piotrowski,E., Thibessard,A. and Leblond,P. (2018) Genome plasticity is governed by double strand break DNA repair in *Streptomyces*. *Sci. Rep.*, **8**, 5272.
36. Bury-Moné,S., Thibessard,A., Lioy,V.S. and Leblond,P. (2023) Dynamics of the *Streptomyces* chromosome: chance and necessity. *Trends Genet.***39**, 873–887.
37. Hoff,G., Bertrand,C., Zhang,L., Piotrowski,E., Chipot,L., Bontemps,C., Confalonieri,F., McGovern,S., Lecointe,F., Thibessard,A., *et al.* (2016) Multiple and variable NHEJ-like genes are involved in resistance to DNA damage in *Streptomyces ambofaciens*. *Front. Microbiol.*, **7**, 1901.
38. McGovern,S., Baconnais,S., Roblin,P., Nicolas,P., Drevet,P., Simonson,H., Piétrement,O., Charbonnier,J.-B., Le Cam,E., Noirot,P., *et al.* (2016) C-terminal region of bacterial Ku controls DNA bridging, DNA threading and recruitment of DNA ligase D for double strand breaks repair. *Nucleic Acids Res.*, **44**, 4785–4806.
39. Bonura,T., Smith,K.C. and Kaplan,H.S. (1975) Enzymatic induction of DNA double-strand breaks in gamma-irradiated *Escherichia coli* K-12. *Proc. Natl. Acad. Sci. U.S.A.*, **72**, 4265–4269.
40. Kuzminov,A. (1995) Instability of inhibited replication forks in *E. coli*. *Bioessays*, **17**, 733–741.
41. Khan,S.R. and Kuzminov,A. (2012) Replication forks stalled at ultraviolet lesions are rescued via RecA and RuvABC protein-catalyzed disintegration in *Escherichia coli*. *J. Biol. Chem.*, **287**, 6250–6265.
42. Raynal,A., Karray,F., Tuphile,K., Darbon-Rongere,E. and Pernodet,J.-L. (2006) Excisable cassettes: new tools for functional analysis of *Streptomyces* genomes. *Appl. Environ. Microbiol.*, **72**, 4839–4844.
43. Gust,B., Challis,G.L., Fowler,K., Kieser,T. and Chater,K.F. (2003) PCR-targeted *Streptomyces* gene replacement identifies a protein domain needed for biosynthesis of the sesquiterpene soil odor geosmin. *Proc. Natl. Acad. Sci. U.S.A.*, **100**, 1541–1546.
44. Luria,S.E. and Delbrück,M. (1943) Mutations of bacteria from virus sensitivity to virus resistance. *Genetics*, **28**, 491–511.
45. Sarkar,S., Ma,W.T. and Sandri,G.H. (1992) On fluctuation analysis: a new, simple and efficient method for computing the expected number of mutants. *Genetica*, **85**, 173–179.
46. Stewart,F.M. (1994) Fluctuation tests: how reliable are the estimates of mutation rates?*Genetics*, **137**, 1139–1146.
47. Hall,B.M., Ma,C.-X., Liang,P. and Singh,K.K. (2009) Fluctuation AnaLysis CalculatOR: a web tool for the determination of mutation rate using Luria–Delbrück fluctuation analysis. *Bioinformatics*, **25**, 1564–1565.
48. Schenk,P.M., Baumann,S., Mattes,R. and Steinbiss,H.H. (1995) Improved high-level expression system for eukaryotic genes in *Escherichia coli* using T7 RNA polymerase and rare ArgtRNAs. *BioTechniques*, **19**, 196–198.
49. Kieser,T. (ed). (2000) In: *Practical Streptomyces genetics Innes*. Norwich.
50. Seemann,T. (2014) Prokka: rapid prokaryotic genome annotation. *Bioinformatics*, **30**, 2068–2069.
51. Tidjani,A.-R., Lorenzi,J.-N., Toussaint,M., van Dijk,E., Naquin,D., Lespinet,O., Bontemps,C. and Leblond,P. (2019) Massive gene flux drives genome diversity between sympatric *Streptomyces* conspecifics. *mBio*, **10**, e01533-19.
52. Goris,J., Konstantinidis,K.T., Klappenbach,J.A., Coenye,T., Vandamme,P. and Tiedje,J.M. (2007) DNA-DNA hybridization values and their relationship to whole-genome sequence similarities. *Int. J. Syst. Evol. Microbiol.*, **57**, 81–91.
53. Darling,A.C.E., Mau,B., Blattner,F.R. and Perna,N.T. (2004) Mauve: multiple alignment of conserved genomic sequence with rearrangements. *Genome Res.*, **14**, 1394–1403.
54. Overbeek,R., Olson,R., Pusch,G.D., Olsen,G.J., Davis,J.J., Disz,T., Edwards,R.A., Gerdes,S., Parrello,B., Shukla,M., *et al.* (2014) The SEED and the rapid annotation of microbial genomes using subsystems technology (RAST). *Nucleic Acids Res.*, **42**, D206–D214.
55. Katoh,K. and Standley,D.M. (2013) MAFFT multiple sequence alignment software version 7: improvements in performance and usability. *Mol. Biol. Evol.*, **30**, 772–780.
56. Choufa,C., Tidjani,A.-R., Gauthier,A., Harb,M., Lao,J., Leblond-Bourget,N., Vos,M., Leblond,P. and Bontemps,C. (2022) Prevalence and mobility of integrative and conjugative elements within a *Streptomyces* natural population. *Front. Microbiol.*, **13**, 970179.
57. Martin,P., Dary,A., André,A., Fischer,G., Leblond,P. and Decaris,B. (1999) Intraclonal polymorphism in the bacterium *Streptomyces ambofaciens* ATCC23877: evidence for a high degree of heterogeneity of the wild type clones. *Mut. Res./Fundam. Mol. Mech. Mutagen.*, **430**, 75–85.

58. Zhang,L., Shi,H., Gan,Q., Wang,Y., Wu,M., Yang,Z., Oger,P. and Zheng,J. (2020) An alternative pathway for repair of deaminated bases in DNA triggered by archaeal NucS endonuclease. *DNA Repair (Amst.)*, **85**, 102734.
59. Zhang,Z., Shitut,S., Claushuis,B., Claessen,D. and Rozen,D.E. (2022) Mutational meltdown of putative microbial altruists in *Streptomyces coelicolor* colonies. *Nat. Commun.*, **13**, 2266.
60. Maslowska,K.H., Makiela-Dzbenska,K., Mo,J.-Y., Fijalkowska,I.J. and Schaaper,R.M. (2018) High-accuracy lagging-strand DNA replication mediated by DNA polymerase dissociation. *Proc. Natl. Acad. Sci. U.S.A.*, **115**, 4212–4217.
61. Simmons,L.A., Davies,B.W., Grossman,A.D. and Walker,G.C. (2008) Beta clamp directs localization of mismatch repair in *Bacillus subtilis*. *Mol. Cell*, **29**, 291–301.
62. Pillon,M.C., Miller,J.H. and Guarné,A. (2011) The endonuclease domain of MutL interacts with the β sliding clamp. *DNA Repair (Amst.)*, **10**, 87–93.
63. Zhang,Y., Yun,K., Huang,H., Tu,R., Hua,E. and Wang,M. (2021) Antisense RNA interference-enhanced CRISPR/Cas9 base editing method for improving base editing efficiency in *Streptomyces lividans* 66. *ACS Synth. Biol.*, **10**, 1053–1063.
64. Amado,L. and Kuzminov,A. (2013) Low-molecular-weight DNA replication intermediates in *Escherichia coli*: mechanism of formation and strand specificity. *J. Mol. Biol.*, **425**, 4177–4191.
65. Rangaswamy,S., Pandey,A., Mitra,S. and Hegde,M.L. (2017) Pre-replicative repair of oxidized bases maintains fidelity in mammalian genomes: the cowcatcher role of NEIL1 DNA glycosylase. *Genes (Basel)*, **8**, 175.
66. Lata,K., Afsar,M. and Ramachandran,R. (2017) Biochemical characterization and novel inhibitor identification of *Mycobacterium tuberculosis* endonuclease VIII 2 (Rv3297). *Biochem. Biophys. Rep.*, **12**, 20–28.
67. Lata,K., Vishwakarma,J., Kumar,S., Khanam,T. and Ramachandran,R. (2022) *Mycobacterium tuberculosis* Endonuclease VIII 2 (Nei2) forms a prereplicative BER complex with DnaN: identification, characterization, and disruption of complex formation. *Mol. Microbiol.*, **117**, 320–333.
68. Ahmad,S., Huang,Q., Ni,J., Xiao,Y., Yang,Y. and Shen,Y. (2020) Functional analysis of the NucS/EndoMS of the Hyperthermophilic Archaeon *Sulfolobus islandicus* REY15A. *Front. Microbiol.*, **11**, 607431.
69. Schaaper,R.M. (1993) Base selection, proofreading, and mismatch repair during DNA replication in *Escherichia coli*. *J. Biol. Chem.*, **268**, 23762–23765.
70. Islam,T. and Josephs,E.A. (2023) Genome editing outcomes reveal mycobacterial NucS participates in a short-patch repair of DNA mismatches. bioRxiv doi: https://doi.org/10.1101/2023.10.23.563644, 23 October 2023, preprint: not peer reviewed.
71. Su,S.S. and Modrich,P. (1986) *Escherichia coli* mutS-encoded protein binds to mismatched DNA base pairs. *Proc. Natl. Acad. Sci. U.S.A.*, **83**, 5057–5061.
72. Lujan,S.A., Clausen,A.R., Clark,A.B., MacAlpine,H.K., MacAlpine,D.M., Malc,E.P., Mieczkowski,P.A., Burkholder,A.B., Fargo,D.C., Gordenin,D.A., *et al.* (2014) Heterogeneous polymerase fidelity and mismatch repair bias genome variation and composition. *Genome Res.*, **24**, 1751–1764.
73. de Paz,A.M., Cybulski,T.R., Marblestone,A.H., Zamft,B.M., Church,G.M., Boyden,E.S., Kording,K.P. and Tyo,K.E.J. (2018) High-resolution mapping of DNA polymerase fidelity using nucleotide imbalances and next-generation sequencing. *Nucleic Acids Res.*, **46**, e78.
74. Batra,V.K., Beard,W.A., Pedersen,L.C. and Wilson,S.H. (2016) Structures of DNA polymerase mispaired DNA termini transitioning to Pre-catalytic complexes support an induced-fit fidelity mechanism.*Structure*, **24**, 1863–1875.
75. Wang,W., Hellinga,H.W. and Beese,L.S. (2011) Structural evidence for the rare tautomer hypothesis of spontaneous mutagenesis. *Proc. Natl. Acad. Sci. U.S.A.*, **108**, 17644–17648.
76. Kimsey,I.J., Petzold,K., Sathyamoorthy,B., Stein,Z.W. and Al-Hashimi,H.M. (2015) Visualizing transient Watson-Crick-like mispairs in DNA and RNA duplexes. *Nature*, **519**, 315–320.
77. Kimsey,I.J., Szymanski,E.S., Zahurancik,W.J., Shakya,A., Xue,Y., Chu,C.-C., Sathyamoorthy,B., Suo,Z. and Al-Hashimi,H.M. (2018) Dynamic basis for dG•dT misincorporation via tautomerization and ionization. *Nature*, **554**, 195–201.
78. Slocombe,L., Al-Khalili,S.J. and Sacchi,M. (2021) Quantum and classical effects in DNA point mutations: watson–Crick tautomerism in AT and GC base pairs. *Phys. Chem. Chem. Phys.*, **23**, 4141–4150.
79. Watson,J.D. and Crick,F.H.C. (1953) Molecular structure of nucleic acids: a structure for deoxyribose nucleic acid. *Nature*, **171**, 737–738.
80. Goodman,M.F. (2018) Smoking gun for a rare mutation mechanism. *Nature*, **554**, 180–181.
81. Sharp,P.M., Shields,D.C., Wolfe,K.H. and Li,W.H. (1989) Chromosomal location and evolutionary rate variation in enterobacterial genes. *Science*, **246**, 808–810.
82. Mira,A. and Ochman,H. (2002) Gene location and bacterial sequence divergence. *Mol. Biol. Evol.*, **19**, 1350–1358.
83. Mei,Q., Fitzgerald,D.M., Liu,J., Xia,J., Pribis,J.P., Zhai,Y., Nehring,R.B., Paiano,J., Li,H., Nussenzweig,A., *et al.* (2021) Two mechanisms of chromosome fragility at replication-termination sites in bacteria. *Sci. Adv.*, **7**, eabe2846.
84. Badel,C., Samson,R.Y. and Bell,S.D. (2022) Chromosome organization affects genome evolution in *Sulfolobus archaea*. *Nat. Microbiol.*, **7**, 820–830.
85. Foster,P.L., Hanson,A.J., Lee,H., Popodi,E.M. and Tang,H. (2013) On the mutational topology of the bacterial genome. *G3*, **3**, 399–407.
86. Niccum,B.A., Lee,H., MohammedIsmail,W., Tang,H. and Foster,P.L. (2019) The symmetrical wave pattern of base-pair substitution rates across the *Escherichia coli* chromosome has multiple causes. *mBio*, **10**, e01226-19.
87. Kivisaar,M. (2019) Mutation and recombination rates vary across bacterial chromosome. *Microorganisms*, **8**, 25.
88. Warnecke,T., Supek,F. and Lehner,B. (2012) Nucleoid-associated proteins affect mutation dynamics in *E. coli* in a growth phase-specific manner. *PLoS Comput. Biol.*, **8**, e1002846.
89. Szafran,M.J., Jakimowicz,D. and Elliot,M.A. (2020) Compaction and control-the role of chromosome-organizing proteins in *Streptomyces*. *FEMS Microbiol. Rev.*, **44**, 725–739.
90. Szafran,M.J., Małecki,T., Strzałka,A., Pawlikiewicz,K., Duława,J., Zarek,A., Kois-Ostrowska,A., Findlay,K.C., Le,T.B.K. and Jakimowicz,D. (2021) Spatial rearrangement of the *Streptomyces venezuelae* linear chromosome during sporogenic development. *Nat. Commun.*, **12**, 5222.
91. Strzałka,A., Kois-Ostrowska,A., Kędra,M., Łebkowski,T., Bieniarz,G., Szafran,M.J. and Jakimowicz,D. (2022) Enhanced binding of an HU homologue under increased DNA supercoiling preserves chromosome organisation and sustains *Streptomyces* hyphal growth. *Nucleic Acids Res.*, **50**, 12202–12216.
92. Henry,C., Kaur,G., Cherry,M.E., Henrikus,S.S., Bonde,N.J., Sharma,N., Beyer,H.A., Wood,E.A., Chitteni-Pattu,S., van Oijen,A.M., *et al.* (2023) RecF protein targeting to post-replication (daughter strand) gaps II: recF interaction with replisomes. *Nucleic Acids Res.*, **51**, 5714–5742.
93. Rivera-Flores,I.V., Wang,E.X. and Murphy,K.C. (2023) *Mycobacterium smegmatis* NucS-promoted DNA mismatch repair involves limited resection by a 5'-3' exonuclease and is independent of homologous recombination and NHEJ. bioRxiv doi: https://doi.org/10.1101/2023.11.26.568737, 26 November 2023, preprint: not peer reviewed.
94. Lioy,V.S., Lorenzi,J.-N., Najah,S., Poinsignon,T., Leh,H., Saulnier,C., Aigle,B., Lautru,S., Thibessard,A., Lespinet,O., *et al.* (2021) Dynamics of the compartmentalized *Streptomyces* chromosome during metabolic differentiation. *Nat. Commun.*, **12**, 5221.

Received: December 21, 2023. **Revised:** January 19, 2024. **Editorial Decision:** February 7, 2024. **Accepted:** February 9, 2024